

Hunting for heavy Z' with IceCube neutrinos and gravitational waves

Basabendu Barman,^{1,*} Arindam Das,^{2,3,†} Suruj Jyoti Das,^{4,‡} and Marco Merchand^{5,6,§}

¹ *Department of Physics, School of Engineering and Sciences, SRM University-AP, Amaravati 522240, India*

² *Institute for the Advancement of Higher Education, Hokkaido University, Sapporo 060-0817, Japan*

³ *Department of Physics, Hokkaido University, Sapporo 060-0810, Japan*

⁴ *Particle Theory and Cosmology Group, Center for Theoretical Physics of the Universe, Institute for Basic Science (IBS), Daejeon, 34126, Korea*

⁵ *KTH Royal Institute of Technology, Department of Physics, SE-10691 Stockholm, Sweden*

⁶ *The Oskar Klein Centre for Cosmoparticle Physics, AlbaNova University Centre, SE-10691 Stockholm, Sweden*

In the minimal gauged B–L extension of the Standard Model, we demonstrate that PeV-scale dark matter (DM) and the baryon asymmetry of the Universe (BAU) can be simultaneously explained through the three right-handed neutrinos (RHNs) present in the theory. The DM candidate undergoes decay into light neutrinos, providing an explanation for the observed IceCube events, while the other two RHNs generate the BAU via leptogenesis. The breaking of gauge symmetry gives rise to detectable gravitational waves (GWs) from decaying cosmic strings (CS), making this framework testable at several future GW detectors—despite being beyond the reach of conventional collider experiments due to the extremely weak coupling. The symmetry-breaking scale establishes a connection between particle masses, couplings, and the GW spectrum, offering a unified and predictive scenario.

Introduction.—Tiny neutrino masses and flavor mixing [1] have been observed from the neutrino oscillation experiments over a period of time. Another significant finding from the PLANCK observation [2] estimates that the baryon asymmetry of the universe (BAU), characterized by the ratio of difference in baryon-antibaryon number density ($n_B - n_{\bar{B}}$) to the entropy density (s), as $Y_B^o \simeq 8.75 \times 10^{-11}$. Additionally, strong evidence for dark matter (DM) comes from astrophysical and cosmological observations, which indicate a relic abundance of $\Omega h^2 \simeq 0.12$ [2–4]. The fundamental origin of these phenomena remains unexplained within the Standard Model (SM), compelling us to explore beyond the SM (BSM) frameworks.

In the recent past, the IceCube neutrino observatory reported the detection of three PeV neutrinos, roughly 3σ excess above the expected background rates [5–9]. These highest-energy events correspond to deposited energies of 1.04 PeV, 1.14 PeV and 2.0 PeV, respectively. Although the origin of these very high energy events is still unclear, it has been shown that such events could be originated from decays of superheavy DM [10–15]. The neutrino energy spectrum presents a high-energy cut-off at half of the DM mass [11, 12] if two body decays including one neutrino are present. Moreover, the IceCube spectrum sets a lower bound on the DM lifetime $\tau_{\text{DM}} \simeq \mathcal{O}(10^{28})$ s [12, 16], which is largely model-independent and significantly exceeds the age of the Universe.

On the other hand, current observations of Gravitational Waves (GWs) [17–23], have opened a complementary avenue to test BSM physics. For example, if symmetries are broken spontaneously at very high temperature then topological defects, such as cosmic strings and domain walls, may appear in the early stages of the universe [24, 25] and the system of these defects can be con-

sidered as a prominent source of a GW background, while the scale of symmetry breaking can be associated with the scale of new physics.

To explore these aspects within a simple yet elegant framework, we consider an extension of the SM featuring an anomaly-free $U(1)_{\text{B-L}}$ gauge group [26, 27], incorporating three generations of SM-singlet right-handed neutrinos (RHNs) and an SM-singlet scalar which acquires a non-zero vacuum expectation value (VEV) resulting in the breaking of the $U(1)_{\text{B-L}}$ symmetry. As a result, the Majorana masses for the RHNs are generated, which in turn induce tiny masses and flavor mixing for the observed left-handed neutrinos via the seesaw mechanism [28–32]. This setup naturally explains the BAU via vanilla leptogenesis if at least two RHN generations contribute to the asymmetry generation, while the third, lightest RHN can serve as a PeV-scale decaying DM candidate, addressing IceCube high-energy neutrino events through the freeze-in mechanism. Additionally, the $U(1)_{\text{B-L}}$ breaking gives rise to one-dimensional topological defects—cosmic strings (CS)—characterized by a string tension $G\mu \sim BGv_\Phi^2$, where v_Φ is the VEV of the $U(1)_{\text{B-L}}$ symmetry breaking singlet scalar and $B \sim 0.1$ [33, 34]. This minimal scenario, therefore, offers a unified explanation for (i) PeV-scale decaying DM linked to IceCube events, (ii) baryogenesis via leptogenesis and (iii) GW from CS which could be tested at future GW detectors. We thus constrain heavy neutral gauge boson mass beyond 1 TeV, with tiny gauge coupling ($\lesssim \mathcal{O}(10^{-5})$), which lies beyond the reach of high energy collider experiments, that typically provide constraints on gauge couplings around $\mathcal{O}(10^{-2})$ for the B–L scenario at the LHC [35].

The framework—Under the $\text{SM} \otimes U(1)_{\text{B-L}}$ gauge symmetry, the SM quark fields transform as $q_L^i = \{3, 2, \frac{1}{6}, \frac{1}{3}\}$,

$u_R^i = \{3, 1, \frac{2}{3}, \frac{1}{3}\}$, $d_R^i = \{3, 1, -\frac{1}{3}, \frac{1}{3}\}$, respectively. The SM lepton fields transform as $\ell_L^i = \{1, 2, -\frac{1}{2}, -1\}$, $e_R^i = \{1, 1, -1, -1\}$, respectively, while the SM Higgs field $H = \{1, 2, \frac{1}{2}, 0\}$. We introduce three SM-singlet RHNs to cancel gauge and mixed gauge-gravity anomalies which transform as $N_R^i = \{1, 1, 0, -1\}$ with $i = 1, 2, 3$ and one SM-singlet $U(1)_{B-L}$ scalar which transforms as $\Phi = \{1, 1, 0, 2\}$. The relevant Yukawa interactions read,

$$\mathcal{L} \supset -Y_{\nu_{\alpha\beta}} \bar{\ell}_L^\alpha \tilde{H} N_R^\beta - \frac{1}{2} Y_{N_\alpha} \Phi (\overline{N_R^\alpha})^c N_R^\alpha + \text{H.c.}, \quad (1)$$

where we start-off in a basis where the Y_{N_α} matrix is diagonal, and $\tilde{H} = i\tau^2 H^*$ with τ^2 being the second Pauli matrix. The scalar potential involving two scalar fields is given by

$$V = \sum_{\mathcal{I}=H,\Phi} \left[m_{\mathcal{I}}^2 (\mathcal{I}^\dagger \mathcal{I}) + \lambda_{\mathcal{I}} (\mathcal{I}^\dagger \mathcal{I})^2 \right] + \lambda_{\text{mix}} (H^\dagger H) (\Phi^\dagger \Phi). \quad (2)$$

After the breaking of B–L and electroweak gauge symmetries, the scalar fields H and Φ develop their VEVs as

$$\langle H \rangle = \frac{1}{\sqrt{2}} \begin{pmatrix} v+h \\ 0 \end{pmatrix}, \quad \text{and} \quad \langle \Phi \rangle = \frac{v_\Phi + \phi}{\sqrt{2}}, \quad (3)$$

where electroweak scale is $v = 246$ GeV at the potential minimum. For $v_\Phi \gg v$, the mass of the B–L gauge boson can be written as $M_{Z'} = 2g_X v_\Phi$. The breaking of B–L symmetry induces the Majorana mass term for the RHNs while the electroweak symmetry breaking generates the Dirac mass term for the light left-handed neutrinos from Eq. (1) as

$$M_\alpha = \frac{Y_{N_\alpha}}{\sqrt{2}} v_\Phi, \quad m_{D_{\alpha\beta}} = \frac{Y_{\nu_{\alpha\beta}}}{\sqrt{2}} v. \quad (4)$$

From the mass matrices above, the light active neutrino masses can be derived using the standard see-saw formula $-m_D M_\alpha^{-1} m_D^T$ [30, 36, 37]. This mechanism successfully explains the tiny neutrino masses and their flavor mixing.

Out of three generations of RHNs, we identify N_1 as a long-lived decaying DM. Its only decay channel, $N_1 \rightarrow \ell H$, produces boosted high-energy neutrinos. The DM lifetime, as required by the IceCube observations, in terms of its mass and Yukawa coupling reads [11, 12, 16, 38]

$$\tau \simeq 10^{28} \text{ s} \left(\frac{(Y_\nu)_{11}}{2 \times 10^{-29}} \right)^2 \left(\frac{M_1}{4 \text{ PeV}} \right). \quad (5)$$

Due to extremely small Yukawa coupling strength, it is not possible to address right DM abundance via the inverse decay channel $\ell H \rightarrow N_1$. Thus, we consider its production via freeze-in [39, 40] from the thermal bath. Consequently, production and decay of N_1 is disentangled, and hence right DM abundance can be satisfied even with a DM decay lifetime of $\tau_{N_1} \sim 10^{28}$ sec, complying with

the IceCube data. Here onward we will consider the following set of parameters as independent in our analysis: $\{g_X, M_{Z'}, Y_{N_\alpha}\}$, while the DM mass ($M_1 = Y_{N_1} v_\Phi / \sqrt{2}$) is always fixed at 4 PeV.

DM production via freeze-in– The PeV scale N_1 DM can be produced via (i) on-shell decay of Z' , provided $M_{Z'} > 2M_1$, (ii) on-shell decay of ϕ , if $m_\phi > 2M_1$ and (iii) 2-to-2 scattering off of the bath particles, mediated by Z' . The universal interaction strength g_X must be feeble to ensure non-thermal DM production via freeze-in (see Sec. II of the supplemental material). As a result, the Z' cannot reach thermal equilibrium, and its comoving number density must be determined by solving a set of coupled Boltzmann equations (BEQs), see Sec. IV of the supplemental material. We consider the mixing between ϕ and the SM Higgs to be negligibly small such that its decay into SM particles are extremely suppressed. Consequently ϕ being a part of the bath and having thermal distribution, it decays dominantly into RHNs and Z' pairs. To fit the observed DM relic density, it is required that $Y_0 M_1 = \Omega h^2 \frac{1}{s_0} \frac{\rho_c}{h^2} \simeq 4.3 \times 10^{-10}$ GeV, where $Y_0 \equiv y_{N_1}(z \rightarrow \infty)$ is the present DM yield. We use the critical energy density $\rho_c \simeq 1.05 \times 10^{-5} h^2 \text{ GeV/cm}^3$, present entropy density $s_0 \simeq 2.69 \times 10^3 \text{ cm}^{-3}$ [41] and DM relic abundance $\Omega h^2 \simeq 0.12$, with $h \simeq H_0/100$ (km/s/Mpc) being the reduced Hubble rate, where $H_0 \simeq 67.4 \pm 0.5$ km/s/Mpc is the current Hubble rate [2].

The evolution of DM and Z' yields ($y_{Z'}$) are shown in the left panel of Fig. 1, as a function of $z = M_1/T$, with $M_1 = 4$ PeV. For the red curves, we fixed $M_{Z'} > 2M_{N_1}$, such that the DM can be produced from the on-shell decay of Z' , as well as via Z' mediated scattering. Now, in presence of both channels, DM production via decay dominates since the production rate is proportional to g_X^2 , compared to scattering, which is proportional to g_X^4 . The DM yield y_{N_1} gradually grows with time, finally reaching the observed abundance in the asymptotic limit. In the first plateau region of the red solid curve, DM is dominantly produced from ϕ -decay. Due to large decay width, ϕ decay is completed earlier and the DM (as well as Z') production from ϕ -decay stops. However, Z' decay still goes on. Thus, the final DM abundance is set by $Z' \rightarrow N_1 N_1$ channel. On the other hand, the blue solid curve represents a scenario where the DM production is instead controlled by Z' mediated scattering, as the decay is kinematically forbidden ($M_{Z'} < M_1$). For $M_{Z'} = 10^8$ (10^5) GeV and for DM mass of 4 PeV, the freeze-in occurs at the temperature $T \sim M_{Z'}$ (M_1). This is the typical IR feature [40], where the DM yield saturates when $T = \max[M_{Z'}, M_1]$.

Baryon asymmetry from N_2 leptogenesis– The observed BAU is generated via vanilla leptogenesis from the CP-violating, out of equilibrium decays of N_2 . Due to very long lifetime, the lepton asymmetry generated through N_1 decay does not contribute to the genera-

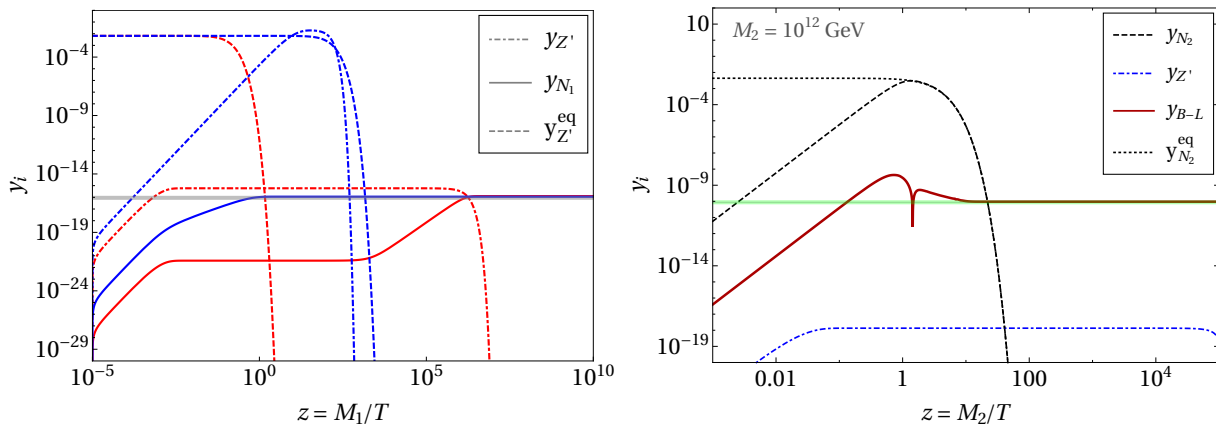


Figure 1. *Left:* Evolution of DM yield (solid curves) with M_1/T . The red and blue curves correspond to $M_{Z'} = \{10^8, 10^5\}$ GeV with corresponding $g_X = \{2 \times 10^{-12}, 1.2 \times 10^{-6}\}$, respectively to produce the right DM abundance (shown via gray thick straight line). In all cases DM mass is fixed to 4 PeV. The equilibrium Z' yield $y_{Z'}^{\text{eq}}$ are shown via the dashed curves. *Right:* Evolution of B–L yield (solid curves) with M_2/T , for N_2 leptogenesis. The red curve produces the observed baryon asymmetry (shown via green thick straight line). The black solid curve shows equilibrium N_2 yield $y_{N_2}^{\text{eq}}$.

tion of the BAU as its decay takes place far below the sphaleron equilibration temperature. The CP asymmetry from N_2 -decay can be expressed as (see Sec. III of the supplemental material) [42, 43]

$$\epsilon_{\Delta L} \simeq \frac{3\delta_{\text{eff}}}{16\pi} \frac{M_2 m_{\nu, \text{max}}}{v^2}, \quad (6)$$

where δ_{eff} is the effective CP violating phase in the neutrino mass matrix with $0 \leq \delta_{\text{eff}} \leq 1$, and, we take $m_{\nu, \text{max}} = 0.05$ eV as the heaviest light neutrino mass following the normal hierarchy. The final B–L asymmetry is obtained by solving a set of coupled BEQs (see Sec. IV of the supplemental material). The sphaleron interactions [42] are in equilibrium within the temperature range 100 GeV to 10^{12} GeV, and they convert a fraction of a non-zero B–L asymmetry into a baryon asymmetry via

$$Y_B \simeq a_{\text{sph}} y_{B-L} = \frac{8N_F + 4N_H}{22N_F + 13N_H} y_{B-L}, \quad (7)$$

where $N_F (= 3)$ and $N_H (= 1)$ are numbers of fermion generations and Higgs doublets, $a_{\text{sph}} \simeq 28/79$ and $Y_B^o \simeq 8.75 \times 10^{-11}$. We show the evolution of yields for RHN (y_{N_2}) and B–L (y_{B-L}) as a function of $z = M_2/T$ in the right panel of Fig. 1. The population of N_2 receives contributions from two sources: (i) the thermal bath, through the inverse decay process $\ell H \rightarrow N_2$ and (ii) decay of Z' and ϕ . Notably, the bath contribution is the dominant one, as all other production channels are suppressed due to tiny g_X to satisfy freeze-in conditions. Following the Davidson-Ibarra (DI) bound [44], $M_2 \gtrsim 10^9$ GeV is required for a successful thermal leptogenesis. Thus, to produce N_2 from on-shell decay of Z' , we need to have $M_{Z'} > 10^9$ GeV, which requires a super-Planckian v_Φ for tiny g_X values. Since the RHN mass depends on

v_Φ from Eq. (4), in order to satisfy DI bound, $v_\Phi \gtrsim 10^9$ GeV for $y_{N_2} \sim \mathcal{O}(1)$, which translates into $g_X \gtrsim 10^{-6}$. This bound on g_X becomes more stringent for $y_{N_2} \lesssim 0.1$.

GW Spectrum from cosmic strings– Numerical simulations based on the Nambu-Goto action [45, 46] have found that for gauged symmetry, the dominant channel of energy loss from CS is through GW radiation from oscillating loops. The rate of energy loss or the power of GW emission is given by [47] $P_{\text{GW}} = \frac{G}{5} (\ddot{Q})^2$, where Q is the quadrupole moment of the oscillating loop, and the triple time derivative $\ddot{Q} \propto \mu$. Thus, the rate of energy loss can be written as $\frac{dE}{dt} = -\Gamma G \mu^2$, where $\Gamma \approx 50$ [48]. Due to GW emission, the loop starts to shrink from its initial length $l_i = \alpha t_i$ at the time of formation (t_i) as $l(t) = \alpha t_i - \Gamma G \mu (t - t_i)$, where α is the loop size parameter and considered to be $\alpha \approx 0.1$ from simulation studies [49, 50]. The total energy loss from a loop constitutes a set of normal mode oscillations with frequencies $f_k = 2k/l(t)$, where k represents number of modes ($k = 1, 2, 3, \dots, \infty$).

The GW density parameter is defined as

$$\Omega_{\text{GW}}(t_0, f) = \frac{f}{\rho_c} \frac{d\rho_{\text{GW}}(t_0, f)}{df} = \sum_k \Omega_{\text{GW}}^{(k)}(t_0, f), \quad (8)$$

where f and t_0 represent the current frequency and the present time, while $\rho_c = 3M_P^2 H_0^2$ is the critical energy density where M_P is reduced Planck mass and Hubble parameter. Since the GW energy density redshifts as a^{-4} , we have [49]

$$\frac{d\rho_{\text{GW}}^{(k)}}{df} = \int_{t_F}^{t_0} \left[\frac{a(t_E)}{a(t_0)} \right]^4 P_{\text{GW}}(t_E, f_k) \frac{dF}{df} dt_E, \quad (9)$$

where f_k denotes emitted frequency (f_E) at the time t_E , t_F is the loop formation time, $\frac{dF}{df} = f \left[\frac{a(t_0)}{a(t_E)} \right]$ accounts

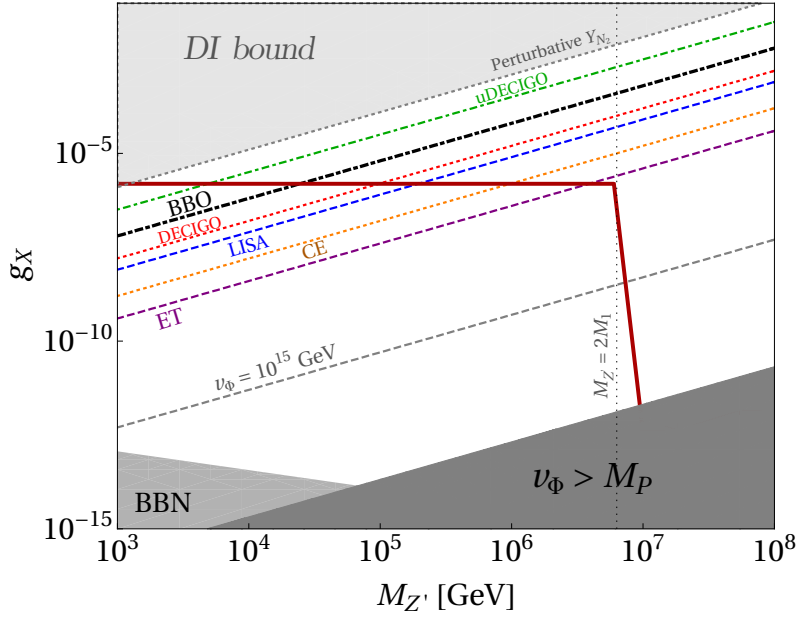


Figure 2. *Summary of parameter space:* The red thick contour corresponds to right DM abundance for $M_1 = 4$ PeV. The diagonal contours correspond to different v_ϕ 's, some of which fall within the sensitivity of a few GW detectors, as denoted. The shaded regions are disallowed from Davidson-Ibarra (DI) bound ($M_2 < 10^9$ GeV), BBN bound on Z' -lifetime and by having super-Planckian VEV-values.

for the redshift of the frequency, and

$$P_{\text{GW}}(t_E, f_k) = \frac{2kG\mu^2\Gamma_k}{f\left[\frac{a(t_0)}{a(t_E)}\right]^2} n\left(t_E, \frac{2k}{f}\left[\frac{a(t_E)}{a(t_0)}\right]\right), \quad (10)$$

is the power emitted by the loops.

The GW spectrum depends on the nature of small-scale structure in the loops which can appear in the form of cusps or kinks [51, 52]. For our study, we consider cusp-like structures to dominate the GW spectra. Here we have $\Gamma_k = \frac{\Gamma k^{-4/3}}{\sum_{m=1}^{\infty} m^{-4/3}}$, with $\sum_k \Gamma_k = \Gamma$ and n denotes the number density of loops which, in a cosmological background with scale factor $a \propto t^\beta$, is found from the Velocity dependent One Scale (VOS) model [53–55] and numerical simulations to be [49]

$$n(t_E, l_k(t_E)) = \frac{A_\beta}{\alpha} \frac{(\alpha + \Gamma G\mu)^{3(1-\beta)}}{[l_k(t_E) + \Gamma G\mu t_E]^{4-3\beta} t_E^{3\beta}}, \quad (11)$$

where A_β is a constant depending on the cosmological background.

Using Eqs. (8)-(11), we obtain the current GW energy density for the mode k as

$$\Omega_{\text{GW}}^{(k)}(t_0, f) = \frac{2kG\mu^2\Gamma_k}{f\rho_c} \int_{t_{\text{osc}}}^{t_0} dt \left[\frac{a(t)}{a(t_0)}\right]^5 n(t, l_k), \quad (12)$$

where the integration over time is from the moment t_{osc} when loops start oscillating after damping due to thermal friction [56] and hence producing sub-dominant effect. For the case of loops formed and radiated during

radiation domination, the GW spectrum has a typical flat plateau, with the amplitude given by

$$\Omega_{\text{GW}}^{(k=1),\text{plateau}}(f) = \frac{128\pi G\mu A_r}{9\zeta(4/3)\epsilon_r} \Omega_r \left[(1 + \epsilon_r)^{3/2} - 1\right] \quad (13)$$

where $\epsilon_r = \alpha/\Gamma G\mu$, and $A_r = 0.54$ [55] for radiation domination. CMB measurements require $G\mu \lesssim 10^{-7}$ [57] and hence we have $\alpha \gg \Gamma G\mu$. This gives $\Omega_{\text{GW}}^{(k=1)}(f) \propto v_\phi$, and hence a higher symmetry breaking scale is more likely to be probed by the GW detectors.

The viable parameter space is furnished in Fig. 2, where the thick red contour corresponds to observed DM abundance for $M_{N_1} = 4$ PeV. The diagonal dashed lines denote different v_ϕ providing the correct value of $M_{Z'}$ for the corresponding g_X . A few of such v_ϕ 's are within the reach of proposed GW detectors: Big Bang Observer (BBO) [58, 59], ultimate DECIGO (uDECIGO) [60, 61], LISA [62], the cosmic explorer (CE) [63] and the Einstein Telescope (ET) [64–67]. The gray shaded region in top left corner is disallowed by the DI bound on the RHN mass for $Y_N \lesssim \sqrt{4\pi}$. The light gray shaded region in the bottom left corner corresponds to the combination of g_X and $M_{Z'}$ that gives rise to $\tau_{Z'} = 1/\Gamma_{Z'} > 1$ sec, thereby jeopardizing the big bang nucleosynthesis (BBN) predictions. The dark gray shaded region in the bottom right corner demands (super-)Planckian v_ϕ . As the $Z' \rightarrow N_1 N_1$ decay channel opens up, one needs $g_X \lesssim 10^{-10}$ to produce the right relic abundance, satisfying the non-thermal condition for freeze-in. As a consequence, the thick red curve takes a sharp bend at

$M_{Z'}/2 = M_1$. For $M_{Z'} < M_1$, final DM yield approximately reads $Y(T_{\text{FI}}) \sim \sigma(T_{\text{FI}}) M_P T_{\text{FI}} \sim g_X^4 M_P/M_1$, where $\sigma(T_{\text{FI}}) \sim g_X^4/T_{\text{FI}}^2$, with freeze-in temperature $T_{\text{FI}} \sim M_1$ as $M_1 > M_{Z'}$. Consequently, the DM abundance becomes almost independent of the mediator mass. Along the red contour, away from the shaded regions, it is always possible to produce the right BAU from N_2 -decay.

Conclusions—We have proposed a scenario that simultaneously accounts for both DM and the BAU while remaining testable at IceCube as well as at several proposed GW detectors. Notably, our approach is broadly applicable to the general class of $U(1)_X$ models. A key element of our framework is the symmetry breaking scale, which unifies all BSM masses and couplings, offering a coherent and compact picture, as illustrated in Fig. 2. This provides bounds on extremely small g_X along with $M_{Z'} \gtrsim 1$ TeV, both lying beyond the reach of standard collider experiments. This work underscores the essential role of multi-messenger astronomy in probing feebly coupled new physics.

Acknowledgments—The work of SJD was supported by IBS under the project code, IBS-R018- D1.

* basabendu.b@srmap.edu.in

† arindamdas@oia.hokudai.ac.jp

‡ surujjd@gmail.com

§ marcomm@kth.se

- [1] **Particle Data Group** Collaboration, S. Navas *et al.*, “Review of particle physics,” *Phys. Rev. D* **110** no. 3, (2024) 030001.
- [2] **Planck** Collaboration, N. Aghanim *et al.*, “Planck 2018 results. VI. Cosmological parameters,” *Astron. Astrophys.* **641** (2020) A6, [arXiv:1807.06209 \[astro-ph.CO\]](#). [Erratum: *Astron. Astrophys.* 652, C4 (2021)].
- [3] G. Bertone and D. Hooper, “History of dark matter,” *Rev. Mod. Phys.* **90** no. 4, (2018) 045002, [arXiv:1605.04909 \[astro-ph.CO\]](#).
- [4] J. de Swart, G. Bertone, and J. van Dongen, “How Dark Matter Came to Matter,” *Nature Astron.* **1** (2017) 0059, [arXiv:1703.00013 \[astro-ph.CO\]](#).
- [5] **IceCube** Collaboration, M. G. Aartsen *et al.*, “First observation of PeV-energy neutrinos with IceCube,” *Phys. Rev. Lett.* **111** (2013) 021103, [arXiv:1304.5356 \[astro-ph.HE\]](#).
- [6] **IceCube** Collaboration, M. G. Aartsen *et al.*, “Evidence for High-Energy Extraterrestrial Neutrinos at the IceCube Detector,” *Science* **342** (2013) 1242856, [arXiv:1311.5238 \[astro-ph.HE\]](#).
- [7] **IceCube** Collaboration, M. G. Aartsen *et al.*, “Observation of High-Energy Astrophysical Neutrinos in Three Years of IceCube Data,” *Phys. Rev. Lett.* **113** (2014) 101101, [arXiv:1405.5303 \[astro-ph.HE\]](#).
- [8] **IceCube** Collaboration, M. G. Aartsen *et al.*, “A combined maximum-likelihood analysis of the high-energy astrophysical neutrino flux measured with IceCube,” *Astrophys. J.* **809** no. 1, (2015) 98, [arXiv:1507.03991 \[astro-ph.HE\]](#).
- [9] **IceCube** Collaboration, M. G. Aartsen *et al.*, “Evidence for Astrophysical Muon Neutrinos from the Northern Sky with IceCube,” *Phys. Rev. Lett.* **115** no. 8, (2015) 081102, [arXiv:1507.04005 \[astro-ph.HE\]](#).
- [10] Y. Bai, R. Lu, and J. Salvado, “Geometric Compatibility of IceCube TeV-PeV Neutrino Excess and its Galactic Dark Matter Origin,” *JHEP* **01** (2016) 161, [arXiv:1311.5864 \[hep-ph\]](#).
- [11] T. Higaki, R. Kitano, and R. Sato, “Neutrino-ful Universe,” *JHEP* **07** (2014) 044, [arXiv:1405.0013 \[hep-ph\]](#).
- [12] A. Esmaili, S. K. Kang, and P. D. Serpico, “IceCube events and decaying dark matter: hints and constraints,” *JCAP* **12** (2014) 054, [arXiv:1410.5979 \[hep-ph\]](#).
- [13] K. Murase, R. Laha, S. Ando, and M. Ahlers, “Testing the Dark Matter Scenario for PeV Neutrinos Observed in IceCube,” *Phys. Rev. Lett.* **115** no. 7, (2015) 071301, [arXiv:1503.04663 \[hep-ph\]](#).
- [14] E. Dudas, T. Gherghetta, K. Kaneta, Y. Mambrini, and K. A. Olive, “Gravitino decay in high scale supersymmetry with R-parity violation,” *Phys. Rev. D* **98** no. 1, (2018) 015030, [arXiv:1805.07342 \[hep-ph\]](#).
- [15] T. Cohen, K. Murase, N. L. Rodd, B. R. Safdi, and Y. Soreq, “ γ -ray Constraints on Decaying Dark Matter and Implications for IceCube,” *Phys. Rev. Lett.* **119** no. 2, (2017) 021102, [arXiv:1612.05638 \[hep-ph\]](#).
- [16] C. A. Argüelles, D. Delgado, A. Friedlander, A. Kheirandish, I. Safa, A. C. Vincent, and H. White, “Dark Matter decay to neutrinos,” [arXiv:2210.01303 \[hep-ph\]](#).
- [17] **LIGO Scientific, Virgo, KAGRA** Collaboration, R. Abbott *et al.*, “Constraints on Cosmic Strings Using Data from the Third Advanced LIGO–Virgo Observing Run,” *Phys. Rev. Lett.* **126** no. 24, (2021) 241102, [arXiv:2101.12248 \[gr-qc\]](#).
- [18] R. Caldwell *et al.*, “Detection of early-universe gravitational-wave signatures and fundamental physics,” *Gen. Rel. Grav.* **54** no. 12, (2022) 156, [arXiv:2203.07972 \[gr-qc\]](#).
- [19] **NANOGrav** Collaboration, G. Agazie *et al.*, “The NANOGrav 15 yr Data Set: Evidence for a Gravitational-wave Background,” *Astrophys. J. Lett.* **951** no. 1, (2023) L8, [arXiv:2306.16213 \[astro-ph.HE\]](#).
- [20] **NANOGrav** Collaboration, A. Afzal *et al.*, “The NANOGrav 15 yr Data Set: Search for Signals from New Physics,” *Astrophys. J. Lett.* **951** no. 1, (2023) L11, [arXiv:2306.16219 \[astro-ph.HE\]](#). [Erratum: *Astrophys. J. Lett.* 971, L27 (2024), Erratum: *Astrophys. J.* 971, L27 (2024)].
- [21] H. Xu *et al.*, “Searching for the Nano-Hertz Stochastic Gravitational Wave Background with the Chinese Pulsar Timing Array Data Release I,” *Res. Astron. Astrophys.* **23** no. 7, (2023) 075024, [arXiv:2306.16216 \[astro-ph.HE\]](#).
- [22] **EPTA, InPTA**: Collaboration, J. Antoniadis *et al.*, “The second data release from the European Pulsar Timing Array - III. Search for gravitational wave signals,” *Astron. Astrophys.* **678** (2023) A50, [arXiv:2306.16214 \[astro-ph.HE\]](#).
- [23] **LISA Cosmology Working Group** Collaboration,

- P. Auclair *et al.*, “Cosmology with the Laser Interferometer Space Antenna,” *Living Rev. Rel.* **26** no. 1, (2023) 5, [arXiv:2204.05434 \[astro-ph.CO\]](#).
- [24] H. B. Nielsen and P. Olesen, “Vortex Line Models for Dual Strings,” *Nucl. Phys. B* **61** (1973) 45–61.
- [25] T. W. B. Kibble, “Topology of Cosmic Domains and Strings,” *J. Phys. A* **9** (1976) 1387–1398.
- [26] A. Davidson, “ $B - L$ as the fourth color within an $SU(2)_L \times U(1)_R \times U(1)$ model,” *Phys. Rev. D* **20** (1979) 776.
- [27] R. E. Marshak and R. N. Mohapatra, “Quark - Lepton Symmetry and B-L as the U(1) Generator of the Electroweak Symmetry Group,” *Phys. Lett.* **91B** (1980) 222–224.
- [28] P. Minkowski, “ $\mu \rightarrow e\gamma$ at a Rate of One Out of 10^9 Muon Decays?,” *Phys. Lett. B* **67** (1977) 421–428.
- [29] T. Yanagida, “Horizontal gauge symmetry and masses of neutrinos,” *Conf. Proc.* **C7902131** (1979) 95–99.
- [30] M. Gell-Mann, P. Ramond, and R. Slansky, “Complex Spinors and Unified Theories,” *Conf. Proc. C* **790927** (1979) 315–321, [arXiv:1306.4669 \[hep-th\]](#).
- [31] R. N. Mohapatra and G. Senjanovic, “Neutrino Mass and Spontaneous Parity Nonconservation,” *Phys. Rev. Lett.* **44** (1980) 912. [231(1979)].
- [32] J. Schechter and J. W. F. Valle, “Neutrino Masses in $SU(2) \times U(1)$ Theories,” *Phys. Rev. D* **22** (1980) 2227.
- [33] A. Babul, T. Piran, and D. N. Spergel, “BOSONIC SUPERCONDUCTING COSMIC STRINGS. 1. CLASSICAL FIELD THEORY SOLUTIONS,” *Phys. Lett. B* **202** (1988) 307–314.
- [34] A. Vilenkin and E. P. S. Shellard, *Cosmic Strings and Other Topological Defects*. Cambridge University Press, 7, 2000.
- [35] A. Das, P. S. B. Dev, Y. Hosotani, and S. Mandal, “Probing the minimal $U(1)_X$ model at future electron-positron colliders via the fermion pair-production channel,” [arXiv:2104.10902 \[hep-ph\]](#).
- [36] O. Sawada and A. Sugamoto, eds., *Proceedings: Workshop on the Unified Theories and the Baryon Number in the Universe: Tsukuba, Japan, February 13-14, 1979*. Natl.Lab.High Energy Phys., Tsukuba, Japan, 1979.
- [37] R. N. Mohapatra and G. Senjanovic, “Neutrino Masses and Mixings in Gauge Models with Spontaneous Parity Violation,” *Phys. Rev. D* **23** (1981) 165.
- [38] M. Chianese and A. Merle, “A Consistent Theory of Decaying Dark Matter Connecting IceCube to the Sesame Street,” *JCAP* **04** (2017) 017, [arXiv:1607.05283 \[hep-ph\]](#).
- [39] L. J. Hall, K. Jedamzik, J. March-Russell, and S. M. West, “Freeze-In Production of FIMP Dark Matter,” *JHEP* **03** (2010) 080, [arXiv:0911.1120 \[hep-ph\]](#).
- [40] N. Bernal, M. Heikinheimo, T. Tenkanen, K. Tuominen, and V. Vaskonen, “The Dawn of FIMP Dark Matter: A Review of Models and Constraints,” *Int. J. Mod. Phys. A* **32** no. 27, (2017) 1730023, [arXiv:1706.07442 \[hep-ph\]](#).
- [41] **Particle Data Group** Collaboration, R. L. Workman *et al.*, “Review of Particle Physics,” *PTEP* **2022** (2022) 083C01.
- [42] W. Buchmuller, P. Di Bari, and M. Plumacher, “Leptogenesis for pedestrians,” *Annals Phys.* **315** (2005) 305–351, [arXiv:hep-ph/0401240](#).
- [43] K. Kaneta, Y. Mambrini, K. A. Olive, and S. Verner, “Inflation and Leptogenesis in High-Scale Supersymmetry,” *Phys. Rev. D* **101** no. 1, (2020) 015002, [arXiv:1911.02463 \[hep-ph\]](#).
- [44] S. Davidson and A. Ibarra, “A Lower bound on the right-handed neutrino mass from leptogenesis,” *Phys. Lett. B* **535** (2002) 25–32, [arXiv:hep-ph/0202239](#).
- [45] C. Ringeval, M. Sakellariadou, and F. Bouchet, “Cosmological evolution of cosmic string loops,” *JCAP* **02** (2007) 023, [arXiv:astro-ph/0511646](#).
- [46] J. J. Blanco-Pillado, K. D. Olum, and B. Shlaer, “Large parallel cosmic string simulations: New results on loop production,” *Phys. Rev. D* **83** (2011) 083514, [arXiv:1101.5173 \[astro-ph.CO\]](#).
- [47] A. Vilenkin, “Gravitational radiation from cosmic strings,” *Phys. Lett. B* **107** (1981) 47–50.
- [48] T. Vachaspati and A. Vilenkin, “Gravitational Radiation from Cosmic Strings,” *Phys. Rev. D* **31** (1985) 3052.
- [49] J. J. Blanco-Pillado, K. D. Olum, and B. Shlaer, “The number of cosmic string loops,” *Phys. Rev. D* **89** no. 2, (2014) 023512, [arXiv:1309.6637 \[astro-ph.CO\]](#).
- [50] J. J. Blanco-Pillado and K. D. Olum, “Stochastic gravitational wave background from smoothed cosmic string loops,” *Phys. Rev. D* **96** no. 10, (2017) 104046, [arXiv:1709.02693 \[astro-ph.CO\]](#).
- [51] T. Damour and A. Vilenkin, “Gravitational wave bursts from cusps and kinks on cosmic strings,” *Phys. Rev. D* **64** (2001) 064008, [arXiv:gr-qc/0104026](#).
- [52] Y. Gouttenoire, G. Servant, and P. Simakachorn, “Beyond the Standard Models with Cosmic Strings,” *JCAP* **07** (2020) 032, [arXiv:1912.02569 \[hep-ph\]](#).
- [53] C. J. A. P. Martins and E. P. S. Shellard, “Quantitative string evolution,” *Phys. Rev. D* **54** (1996) 2535–2556, [arXiv:hep-ph/9602271](#).
- [54] C. J. A. P. Martins and E. P. S. Shellard, “Extending the velocity dependent one scale string evolution model,” *Phys. Rev. D* **65** (2002) 043514, [arXiv:hep-ph/0003298](#).
- [55] P. Auclair *et al.*, “Probing the gravitational wave background from cosmic strings with LISA,” *JCAP* **04** (2020) 034, [arXiv:1909.00819 \[astro-ph.CO\]](#).
- [56] A. Vilenkin, “Cosmic string dynamics with friction,” *Phys. Rev. D* **43** (1991) 1060–1062.
- [57] T. Charnock, A. Avgoustidis, E. J. Copeland, and A. Moss, “CMB constraints on cosmic strings and superstrings,” *Phys. Rev. D* **93** no. 12, (2016) 123503, [arXiv:1603.01275 \[astro-ph.CO\]](#).
- [58] J. Crowder and N. J. Cornish, “Beyond LISA: Exploring future gravitational wave missions,” *Phys. Rev. D* **72** (2005) 083005, [arXiv:gr-qc/0506015](#).
- [59] V. Corbin and N. J. Cornish, “Detecting the cosmic gravitational wave background with the big bang observer,” *Class. Quant. Grav.* **23** (2006) 2435–2446, [arXiv:gr-qc/0512039](#).
- [60] N. Seto, S. Kawamura, and T. Nakamura, “Possibility of direct measurement of the acceleration of the universe using 0.1-Hz band laser interferometer gravitational wave antenna in space,” *Phys. Rev. Lett.* **87** (2001) 221103, [arXiv:astro-ph/0108011](#).
- [61] H. Kudoh, A. Taruya, T. Hiramatsu, and Y. Himemoto, “Detecting a gravitational-wave background with next-generation space interferometers,” *Phys. Rev. D* **73** (2006) 064006, [arXiv:gr-qc/0511145](#).
- [62] **LISA** Collaboration, P. Amaro-Seoane *et al.*, “Laser

- Interferometer Space Antenna,” [arXiv:1702.00786](#) [[astro-ph.IM](#)].
- [63] D. Reitze *et al.*, “Cosmic Explorer: The U.S. Contribution to Gravitational-Wave Astronomy beyond LIGO,” *Bull. Am. Astron. Soc.* **51** no. 7, (2019) 035, [arXiv:1907.04833](#) [[astro-ph.IM](#)].
- [64] S. Hild *et al.*, “Sensitivity Studies for Third-Generation Gravitational Wave Observatories,” *Class. Quant. Grav.* **28** (2011) 094013, [arXiv:1012.0908](#) [[gr-qc](#)].
- [65] M. Punturo *et al.*, “The Einstein Telescope: A third-generation gravitational wave observatory,” *Class. Quant. Grav.* **27** (2010) 194002.
- [66] B. Sathyaprakash *et al.*, “Scientific Objectives of Einstein Telescope,” *Class. Quant. Grav.* **29** (2012) 124013, [arXiv:1206.0331](#) [[gr-qc](#)]. [Erratum: *Class.Quant.Grav.* 30, 079501 (2013)].
- [67] M. Maggiore *et al.*, “Science Case for the Einstein Telescope,” *JCAP* **03** (2020) 050, [arXiv:1912.02622](#) [[astro-ph.CO](#)].

Supplemental Material

I. RELEVANT DECAY WIDTHS AND CROSS-SECTIONS

The partial decay width of Z' into a pair of single generation SM fermions and DM reads,

$$\Gamma_{Z' \rightarrow f_i \bar{f}_i} = N_c \frac{g_X^2 M_{Z'}}{24\pi} \left[(Q_L^2 + Q_R^2) \right], \quad \Gamma_{Z' \rightarrow N_1 N_1} = \frac{g_X^2 M_{Z'}}{24\pi} \left(1 - \frac{4M_1^2}{M_{Z'}^2} \right)^{\frac{3}{2}} \quad (14)$$

where $N_c = 1(3)$ is the color factor for leptons (quarks) and $Q_{L(R)}$ is the B–L charge for the left(right handed) SM fermions, and we have taken the limit in which $M_{Z'}$ is much heavier compared to the SM particles.

The dominant decay rates of ϕ are given by,

$$\Gamma_{\phi \rightarrow Z' Z'} = \frac{g_X^2}{8\pi r^4} \frac{M_{Z'}^2}{m_\phi} \sqrt{1 - 4r^2} (12r^4 - 4r^2 + 1), \quad \Gamma_{\phi \rightarrow N_i N_i} = \frac{g_X^2}{2\pi} \left(\frac{M_i}{M_{Z'}} \right)^2 m_\phi \left(1 - \frac{4M_i^2}{m_\phi^2} \right)^{3/2} \quad (15)$$

where $r = M_{Z'}/m_\phi$.

For very heavy Z' and DM, the total annihilation cross-section mediated by Z' reads,

$$\sigma(s)_{\text{SM SM} \rightarrow N_1 N_1} = \frac{170 g_X^4}{2592 \pi} \frac{s}{\left[(s - M_{Z'}^2)^2 + \Gamma_{Z'}^2 M_{Z'}^2 \right]} \left(1 - \frac{4M_1^2}{s} \right)^{3/2} \quad (16)$$

where $\Gamma_{Z'}$ is the total decay width of Z' into all possible final states.

II. DARK MATTER PRODUCTION RATE

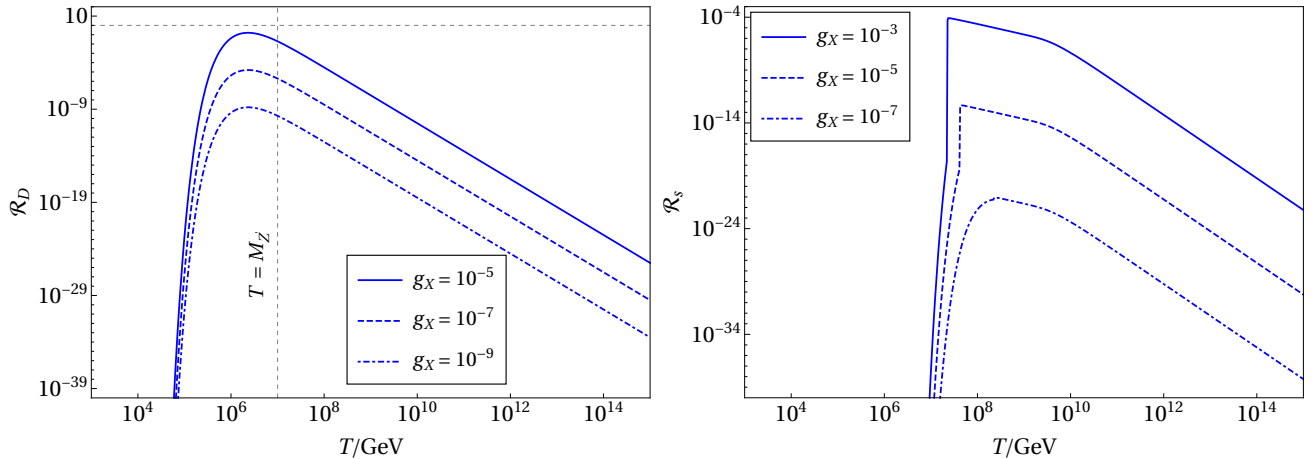


Figure 3. *Left*: DM production rate from Z' decay, as a function of the bath temperature T , for different choices of g_X . Here we have fixed $M_{Z'} = 10^7$ GeV. *Right*: Same as left, but considering DM production from 2-to-2 scattering, mediated by Z' , where $M_{Z'} = 10^5$ GeV. In all cases the DM mass is fixed at 4 PeV.

The DM production rate from Z' decay is given by the production rate densities as

$$\gamma_D = \frac{g_a}{2\pi^2} m_a^2 \Gamma_{Z' \rightarrow N_1 N_1} T K_1 \left(\frac{m_a}{T} \right), \quad (17)$$

while production from 2-to-2 scattering off of the bath particles reads

$$\gamma_s = \frac{T}{32\pi^4} g_a g_b \times \int_{\max[(m_a+m_b)^2, 4M_1^2]}^{\infty} ds \frac{\left[(s - m_a^2 - m_b^2)^2 - 4m_a^2 m_b^2 \right]}{\sqrt{s}} \sigma(s)_{a,b \rightarrow N_1 N_1} K_1 \left(\frac{\sqrt{s}}{T} \right). \quad (18)$$

Here, the subindices a, b correspond to the SM states, $g_{a,b}$ are the corresponding degrees of freedom and K_i denotes the modified Bessel functions of i^{th} kind. In order to ensure out of equilibrium DM production, the following condition needs to be satisfied

$$\mathcal{R}_i \equiv \frac{\gamma_i}{n_{\text{eq}}^{N_1} H} < 1, \quad (19)$$

where H is the Hubble parameter during radiation domination and $n_{\text{eq}} = (T/(2\pi^2)) m^2 K_2(m/T)$ is the equilibrium number density. Note that, here we use the equilibrium number density for the DM itself in order to obtain the conservative bound on the masses and couplings. In Fig. 3 we show the evolution of DM production rate, as a function of the temperature of the thermal bath. Due to g_X^2 dependence, it is not possible to have $g_X \gtrsim 10^{-4}$ in order to ensure $\mathcal{R} < 1$ till $T \simeq M_{Z'}$ in the case of DM genesis via decay. However, for scattering it is still possible to have g_X as large as about 10^{-3} , while ensuring $\mathcal{R} < 1$ because of the g_X^4 dependence of the scattering cross-section. Note that, in this case the DM production starts at $T \sim M_1$, as prior to that the thermal bath is not energetic enough to produce such a massive DM.

III. CP-ASYMMETRY FROM N_2 DECAY

Since N_1 is a long-lived DM, the CP asymmetry generated from N_2 decay is given by

$$\epsilon_{\Delta L} \equiv \frac{\Gamma_{N_2 \rightarrow \ell_i H} - \Gamma_{N_2 \rightarrow \bar{\ell}_i \bar{H}}}{\Gamma_{N_2 \rightarrow \ell_i H} + \Gamma_{N_2 \rightarrow \bar{\ell}_i \bar{H}}} \simeq \frac{1}{8\pi} \frac{1}{(Y_\nu^\dagger Y_\nu)_{22}} \text{Im}(Y_\nu^\dagger Y_\nu)_{23}^2 \times \mathcal{F}\left(\frac{M_3^2}{M_2^2}\right), \quad (20)$$

where

$$\mathcal{F}(x) \equiv \sqrt{x} \left[\frac{1}{1-x} + 1 - (1+x) \log\left(\frac{1+x}{x}\right) \right]. \quad (21)$$

For $x \gg 1$, $\mathcal{F} \simeq -3/(2\sqrt{x})$, and Eq. (20) becomes

$$\epsilon_{\Delta L} \simeq -\frac{3}{16\pi} \frac{1}{(Y_\nu^\dagger Y_\nu)_{22}} \times \left[\text{Im}(Y_\nu^\dagger Y_\nu)_{23}^2 \right] \frac{M_2}{M_3}. \quad (22)$$

Then

$$\epsilon_{\Delta L} \simeq -\frac{3 \delta_{\text{eff}} |(Y_\nu)_{23}|^2 M_2}{16\pi M_3}, \quad (23)$$

while the effective CP violating phase is given by

$$\delta_{\text{eff}} = \frac{1}{(Y_\nu)_{23}^2} \frac{\text{Im}(Y_\nu^\dagger Y_\nu)_{23}^2}{(Y_\nu^\dagger Y_\nu)_{22}}. \quad (24)$$

To connect with the light neutrino mass, we impose the seesaw relation

$$m_{\nu,3} = \frac{|(Y_\nu)_{23}|^2 v^2}{M_1}, \quad (25)$$

which corresponds to the heaviest left-handed neutrino in the normal hierarchy. This leads to

$$\epsilon_{\Delta L} \simeq -\frac{3 \delta_{\text{eff}} M_2 m_{\nu,3}}{16\pi v^2}. \quad (26)$$

IV. BOLTZMANN EQUATIONS

For freeze-in

The coupled BEQs for freeze-in production of the DM, N_1 , read

$$\begin{aligned} \frac{dy_\phi}{dz} &= -\frac{z}{\mathcal{H}} \langle \Gamma_\phi \rangle y_{\text{eq}}^\phi + \frac{s}{\mathcal{H}} \frac{1}{z^2} \langle \sigma v \rangle_{\text{SM SM} \rightarrow \phi \phi} (y_{\text{eq}}^\phi)^2, \\ \frac{dy_{Z'}}{dz} &= -\frac{z}{\mathcal{H}} \langle \Gamma_{Z'} \rangle y_{Z'} + \frac{z}{\mathcal{H}} \langle \Gamma_{\phi \rightarrow Z' Z'} \rangle (y_{\text{eq}}^\phi - y_{Z'}), \\ \frac{dy_{N_1}}{dz} &= \frac{z}{\mathcal{H}} \langle \Gamma_{Z' \rightarrow N_1 N_1} \rangle y_{Z'} + \frac{z}{\mathcal{H}} \langle \Gamma_{\phi \rightarrow N_1 N_1} \rangle y_{\text{eq}}^\phi + \frac{s}{\mathcal{H}} \frac{1}{z^2} \langle \sigma v \rangle_{\text{SM SM} \rightarrow N_1 N_1} y_{\text{eq}}^2, \end{aligned} \quad (27)$$

where $y_i \equiv n_i/s$ is the yield of a certain species i , with

$$y_j^{\text{eq}} = \frac{45}{4\pi^4} \frac{g_j}{g_{*s}} z^2 K_2[z], \quad (28)$$

is the equilibrium yield, with g_j being the degrees of freedom for the corresponding j particle and $z = M_1/T$ is a dimensionless variable. Here, $\mathcal{H} = (\pi/3) \sqrt{g_*/10} (T^2/M_P)$ is the Hubble parameter for a standard radiation dominated (RD) Universe and $s = (2\pi^2/45) g_{*s}(T) T^3$ is the entropy density. The number of relativistic degrees of freedom in the bath corresponding to energy density and entropy density are tracked by $g_*(T)$ and $g_{*s}(T)$, respectively. At temperatures well above the QCD phase transition we have $g_*(T) \simeq g_{*s}(T) \approx 106$. The first line of Eq. (27) corresponds to the yield of ϕ , with Γ_ϕ being its decay rate as reported in Appendix. I, where the thermally averaged decay rate is given by

$$\langle \Gamma_{\phi \rightarrow jj} \rangle = \frac{K_1(z)}{K_2(z)} \times \Gamma_{\phi \rightarrow jj}, \quad (29)$$

with $z = M_1/T$, and j represents the final state particle. The second line of Eq. (27) takes care of the Z' yield, sourced from the decay of ϕ . Finally, in the third line, we provide the evolution equation for DM yield, sourced from Z' -decay, ϕ -decay and Z' -mediated scattering channels.

For baryon asymmetry

To track the evolution of RHN number density and the corresponding B–L asymmetry with time, we solve the following set of BEQs (along with the first one in Eq. (27)),

$$\begin{aligned} \frac{dy_{Z'}}{dz} &= -\frac{z}{\mathcal{H}} \langle \Gamma_{Z'} \rangle y_{Z'} + \frac{z}{\mathcal{H}} \langle \Gamma_{\phi \rightarrow Z' Z'} \rangle (y_{\text{eq}}^\phi - y_{Z'}) \\ \frac{dy_{N_2}}{dz} &= \frac{z}{\mathcal{H}} \langle \Gamma_{Z' \rightarrow N_2 N_2} \rangle y_{Z'} + \frac{z}{\mathcal{H}} \langle \Gamma_{\Phi \rightarrow N_2 N_2} \rangle y_{\text{eq}}^\phi + \frac{s}{\mathcal{H}} \frac{1}{z^2} \langle \sigma v \rangle_{\text{SM SM} \rightarrow N_2 N_2} (y_{N_2}^{\text{eq}^2} - y_{N_2}^2) - \frac{z}{\mathcal{H}} \langle \Gamma_{N_2} \rangle (y_{N_2} - y_{N_2}^{\text{eq}}) \\ \frac{dy_{B-L}}{dz} &= \frac{\langle \Gamma_{N_2} \rangle}{\mathcal{H}} z \epsilon_{\Delta L} (y_{N_2} - y_{N_2}^{\text{eq}}) - \frac{\langle \Gamma_{N_2} \rangle}{\mathcal{H}} \frac{z^3}{4} \frac{\tilde{m}_2}{m_*} K_1(z) y_{B-L} \end{aligned} \quad (30)$$

where $z = M_2/T$. Once again, the first line of the set of equations above takes into account the production of Z' from the thermal bath, via the decay of ϕ and the decay of Z' into several final states. The second line corresponds to the evolution of N_2 yield. The produced N_2 's then undergo CP violating out of equilibrium decay producing a net B–L asymmetry. The evolution of this asymmetry is tracked by the last line of the equation, where we also include the contribution of inverse decays to the washout term. Here, $\tilde{m}_2 = (m_D^\dagger m_D)_{22}/M_2 \approx m_{\nu,2}^2/M_2$ and $m_* \simeq 10^{-3}$ eV is the equilibrium neutrino mass [42]. In our scenario, we find, $\tilde{m}_2 > m_*$, as a result we are always in the strong washout regime. Thermally averaged N_2 decay width is given by

$$\langle \Gamma_{N_2} \rangle = \frac{K_1(M_2/T)}{K_2(M_2/T)} \frac{M_2}{4\pi} \frac{m_{\nu,2} M_2}{v^2}. \quad (31)$$

In the second line we have utilized the seesaw relations, where, following normal hierarchy, $m_{\nu,1} \simeq 0$, $m_{\nu,2} \simeq 0.0086$ eV and $m_{\nu,3} \simeq 0.0506$ eV.